Annals of Glaciology 27 1998

The effects of ocean warming on melting and ocean circulation under the Amery Ice Shelf, East Antarctica

M. J. M. Williams,[1] R. C. Warner,[2] W. F. Budd[2]
[1]*Antarctic CRC and IASOS, University of Tasmania, Box 252-80, Hobart, Tasmania 7001, Australia*
[2]*Antarctic CRC, Box 252-80, Hobart, Tasmania 7001, Australia*

ABSTRACT. Using a three-dimensional ocean model specially adapted to the ocean cavity under the Amery Ice Shelf, we investigated the present ocean circulation and pattern of ice-shelf basal melting and freezing, the differences which would result from temperature changes in the seas adjacent to the Amery Ice Shelf, and the ramifications of these changes for the mass balance of the ice shelf. Under present conditions we estimate the net loss from the Amery Ice Shelf from excess basal melting over freezing at approximately 7.8 Gt a^{-1}. This comprises a gross loss of 11.4 Gt a^{-1} at a mean rate of 0.42 m a^{-1}, which is partially offset by freezing-on of 3.6 Gt a^{-1}, at a mean rate of 0.19 m a^{-1}. When the adjacent seas were assumed to warm by 1 °C, we found the net melt increased to 31.6 Gt a^{-1}, comprising 34.6 Gt a^{-1} of gross melt and 3.0 Gt a^{-1} of freezing.

INTRODUCTION

The ice shelves which surround much of the Antarctic coastline are important components of the global climate system, as they allow rapid interaction between the Antarctic ice sheet and the world's oceans. Basal melting from these ice shelves could account for approximately 20% of the ablation of the Antarctic ice sheet (Jacobs and others, 1992), and is a key ingredient in driving the ocean circulation within the cavities underlying the larger ice shelves. The Amery Ice Shelf is the third largest embayed ice shelf, and forms the floating portion of the Lambert Glacier system, a glacier system which drains a large part of the East Antarctic ice sheet. Therefore, basal melting from the Amery Ice Shelf may be a significant source of ice loss from the Lambert Glacier system. In this paper we present an estimate of the amount of ice lost from the Amery Ice Shelf via basal melting, and examine how this changes under different ocean–climate scenarios.

A two-dimensional vertical plane-flow model was previously applied (Hellmer and Jacobs, 1992) to the ocean cavity under the Amery Ice Shelf. Hellmer and Jacobs studied several different configurations of the ocean domain, and in all cases, except with their channel-flow model, found an overturning circulation, driven by melt at the ice–ocean interface. The channel-flow model was used to simulate the three-dimensional flow, expressing inflow on the east side of the Amery Ice Shelf and outflow on the west side of the domain. These were connected so as to allow flow near the grounding line at the south of the domain. From the channel flow, they found melting rates of −0.3 m a^{-1} (freezing) to 2.7 m a^{-1} (melting).

In this study of the Amery Ice Shelf we use the same three-dimensional sub-ice-shelf ocean model as Determann and Gerdes (1994) and Determann and others (1994), as this is expected to provide a better description of the ocean dynamics than alternate models (Williams and others, 1998). After tailoring the three-dimensional ocean model to the ocean cavity under the Amery Ice Shelf, we were able to examine the effects of a global ocean-warming scenario on both ocean circulation and basal melting. Global warming was simulated by modifying the potential temperature along the open northern boundary of the model, from present conditions. For the model runs, the salinity profiles remained unchanged, with a mean of 34.37‰. The present mean temperature along the boundary is −1.56 °C. The temperature along the whole boundary was increased in different runs by 0.1–1.0 °C. This is less than the increase suggested from global climate models which, for a trebling of CO_2, suggest temperature changes along the Antarctic coast on the order of 1.5 °C (O'Farrell and others, 1997). We also examined the effects of cooling the water along the northern boundary. At each depth level the amount of cooling was determined from the difference between the present temperature and the surface freezing temperature for the present salinity. If this difference was less than 1 °C, we used the surface freezing temperature; if greater than 1 °C we cooled the present temperatures by 1 °C; and where the present temperature was less than the surface freezing temperature, it remained at the present temperature. The mean change in the temperature on the whole water column on the boundary was ~−0.19 °C. At depths below the minimum ice-shelf draft at the boundary the mean temperature change was ~−0.03 °C, with a maximum change of ~−0.15 °C.

MODEL DESCRIPTION

The circulation in sub-ice-shelf ocean cavities is a distinctive problem in ocean modelling because the ice shelf insulates the ocean from the effects of atmospheric interaction, provides an inclined topography at the top of the water column and, most importantly, provides direct surface forcing to the ocean. In addition, the basal ice-mass exchange has a significant effect on the mass balance of the ice shelf.

https://doi.org/10.3189/1998AoG27-1-75-80 Published online by Cambridge University Press

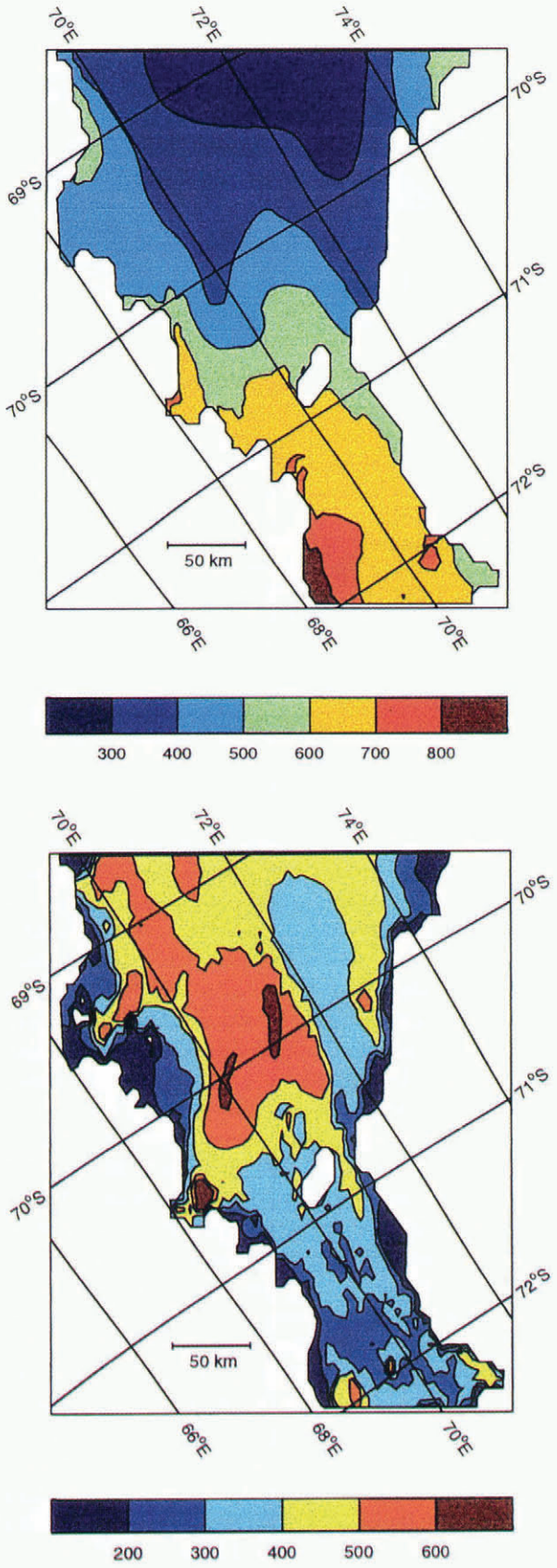

Fig. 1. (a) Ice-shelf draft, and (b) water-column thickness, over the model domain. Thicknesses are in metres.

The ocean model used here was originally applied to a sub-ice-shelf circulation by Determann and Gerdes (1994). The model is a three-dimensional, primitive equation model based on the work of Bryan (1969) and Cox (1984), which has been adapted to σ coordinates (Gerdes, 1993), where σ equals the depth below the ice-shelf base divided by the water-column thickness. The advantage of using σ coordinates, is that they allow for convenient specification of kinematic boundary conditions both at the interface between the ice shelf and the ocean and on the seabed (these are the top and bottom model coordinate surfaces). The model derives the horizontal velocity components, potential temperature, salinity and additional passive tracers. Vertical velocity is calculated from the continuity equation for an incompressible fluid. Sub-grid-scale mixing processes within the water column are parameterised using the conventional eddy-viscosity/diffusivity formulation with constant coefficients.

For the present application the model has ten σ layers, with layer thicknesses varying from ~2% of the water-column thickness in the top layer, to ~23% of the water-column thickness in the bottom layer. In the horizontal coordinates we used a latitude–longitude grid rotated by 12° with a spacing of 0.05° by 0.1°, which gives an approximate resolution of 5.5 km by 4.3 km. During model spin-up and after it reached equilibrium the model was forced along the northernmost boundary and at the ice-shelf/ocean interface. The parameterisation of the forcing at the ice-shelf/ocean interface is described in Determann and Gerdes (1994).

The northern ocean boundary, which runs along a smoothed Amery Ice Front, is forced by a temperature and salinity field based on hydrographic observations in Prydz Bay, near the ice front (Wong, 1994). Along this boundary the model distinguishes between inflow and outflow using the cross-boundary velocity field. This effectively allows outflowing water to leave the cavity, without the temperature or salinity of the outflowing waters having any effect on the inflowing water masses. In areas of inflow the interior temperature and salinity are relaxed over a time period of 80 days to the Prydz Bay temperature and salinity fields.

The shape of the ocean cavity under the ice shelf is characterised by the water-column thickness and the ice-shelf draft. The ice-shelf draft presented in Figure 1a is derived from unpublished radar ice-thickness observations (personal communication from I. Allison, 1996), while the water-column thickness (Fig. 1b) is derived from the difference between the ice-shelf draft and the seabed. The seabed topography was taken from mapping based on seismic observations presented in Kurinin and Aleshkova (1987). Some features have been lost where the water column would be less than the 50 m required for the ten σ layers, or where there were insufficient horizontal gridpoints to resolve small features.

PRESENT CONDITIONS

Ocean circulation

Here we concentrate on the horizontal circulation and its response to the climate-change forcing; further details of the sub-ice-shelf oceanography will be presented elsewhere. The ocean circulation was found to be generally vertically coherent through the water column. The dominant feature of this circulation (Fig. 2) is the clockwise rotating gyre near the centre of the domain. Around the Central Gyre (labelled CG in Fig. 2) are five other major labelled features of the flow. These are the Northern Gyre (NG), the Northeastern Gyre (NEG), the Southeastern Gyre (SEG), the Southwestern Gyre (SWG) and the Western Boundary

https://doi.org/10.3189/1998AoG27-1-75-80 Published online by Cambridge University Press

Current (WBC). The majority of these features in the circulation are topographically trapped. In particular the CG is trapped, to the north and east by the seabed topography and to the south and west by the ice-shelf draft.

Along the northern boundary of the domain, cross-boundary flow is very dependent on the water-column thickness. The flow is generally vertically coherent, although in areas where inflow occurs flow is stronger near the seabed, while in outflow areas it is stronger near the base of the ice shelf. The largest area of inflow is in a deep trench which runs to the east of the 70.0° E meridian (Fig. 1b). Weaker inflows occur near 74.0° E, where the ice shelf thickens sharply, and at around 72.0° E.

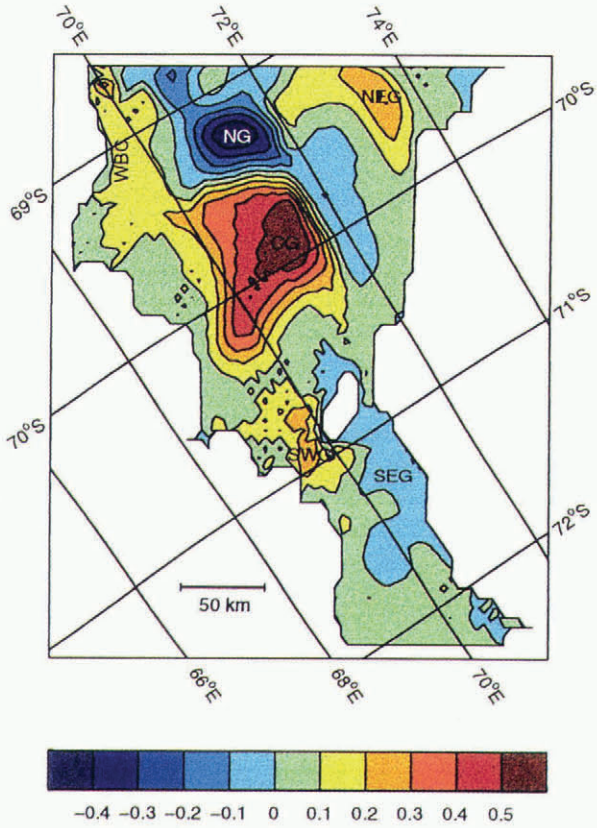

Fig. 2. Present vertically integrated stream function (Sv). The letter codes indicate key features of the circulation and are described in the text. Circulation is clockwise around positive features.

Most of the inflow from the two western inflow regions is collected in the NG. The flow from the region near 72.0° E, circulates through the western side of the NG, where it is joined by flow along the base of the deep trench. From here the flow divides, with the bulk of the flow going east and then south as part of the CG. The smaller amount recirculates, flowing back towards the boundary, where the flow divides again. Some flows out of the domain at about 73.0° E, some turns to the east and joins the NEG, while the rest remains in the NG.

After joining the NEG, the flow is parallel to the boundary, before combining with the third major source of inflow. Here it turns to the south, following the water-column thickness contours. The western side of the NEG bounds an area of weak northward flow, through an area of relatively constant ice-shelf draft and water-column thickness.

The CG is the dominant source of north–south movement of water, with a total transport of ~0.61 Sv (1 Sv = 1×10^6 m^3 s^{-1}). It transports water warmer than the in situ freezing temperature south, then brings cooled water north near the western boundary. This helps drive the WBC, which when it reaches the northern boundary, is the largest outflow.

The other areas of outflow, which sit between the areas of inflow, have peak velocities that are less than one-third that of the outflowing WBC.

South of the Central Grounded Zone the circulation can be described in terms of the SEG and SWG. Water enters the southern part of the domain, along the west side of the Central Grounded Zone, where it turns slightly to the east before heading south. Once at the southern end of the domain the flow divides, with return flow up the eastern and western sides of the southern part of the domain. The eastern boundary flow is generally broad and weak, but strengthens as it flows north through the channel to the east of the Central Grounded Zone.

In contrast, the flow up the western boundary is relatively restricted in extent. After reconnecting with the strongest part of the SWG the current continues north, forming the basis of the WBC.

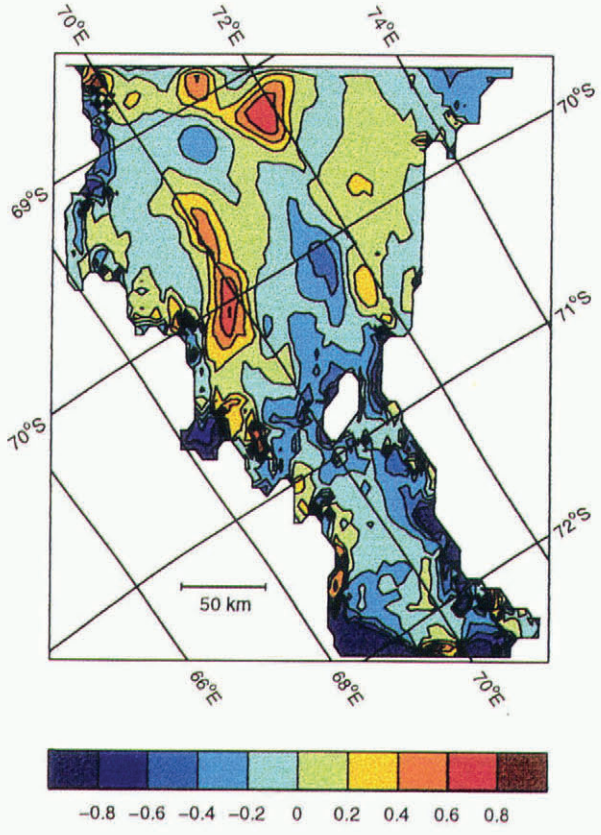

Fig. 3. Present distribution of rates of melting and freezing. Rates are in m a^{-1}, and positive values indicate freezing.

Rates of melting and freezing

The distribution of ice-shelf basal melting and freezing rates (Fig. 3) shows clear division between the areas where melting occurs (−) and the areas where freezing occurs (+). This distribution is largely determined by the depth of the ice shelf, with most of the divergence from the expected pattern (melting where the ice shelf is thickest, and freezing where

https://doi.org/10.3189/1998AoG27-1-75-80 Published online by Cambridge University Press

the ice shelf is thinnest) apparently related to the advective effects of the ocean circulation.

The highest rates of melting occur where we expect them, in the southeast and southwest of the domain where the ice shelf is thickest. High rates of melting can also occur in areas where the ice-shelf thickness is not the determining factor. In these areas (e.g. east of the Central Grounded Zone, and around 70.1° S, 71.5° E) steep ice-shelf draft gradients cause warm water to outcrop into the top layer and drive the melting.

In contrast, the areas of freezing seem to be more closely linked to the underlying ocean circulation. The three regions of extensive freezing are in areas where water cooled at depth is flowing north, still in contact with the ice shelf. The strongest of these regions is coupled to the western side of the CG and extends towards the outflow of the WBC. The cooled water which drives this freezing is supplied from four sources: the area of strong melt around 70.5° S, 68.5° E, the area of melting coupled to the eastern side of the CG, the area of melting coupled to the western side of the NG, and south of the Central Grounded Zone. The broad area of freezing in the northeast of the domain is supplied with supercooled water, from the south of the domain, via the channel to the east of the Central Grounded Zone, the eastern margin of the CG, and to a lesser extent from melting in the northeast corner of the domain. The third area of significant freezing, in the north of the domain, is interesting because supercooled water from its main source, south of the Central Grounded Zone, has to flow through another area of intensive freezing (the northeastern area). The only local source, the melting area coupled to the western portion of the NG, has insufficient melting to be the main source, but still contributes.

The smaller, localised areas of freezing, particularly in the south of the domain, where the ice shelf is still comparatively thick, are caused by the same mechanism that generates the high freezing rates within the significant areas of freezing, i.e. steep local ice-shelf gradients. These allow the rapid rise of supercooled water, which drives high freezing rates.

RESPONSE TO OCEAN TEMPERATURE CHANGE

Very little change occurs in the ocean circulation when the boundary temperatures are cooled. Under the warming scenarios examined, the changes in some features of the circulation are significant. In the south of the domain, both the SEG and the SWG shift. The SWG moves to the north, merging with the southern end of the CG, and after +0.1°C of warming is no longer distinguishable as a separate gyre. The core of the SEG initially moves to the west and reduces in extent. Then, as the warming increases, the SEG becomes more distinct, and strengthens from around 0.05 Sv under present conditions to 0.4 Sv in the 1.0°C warming scenario.

North of the Central Grounded Zone the significant changes in the circulation for the warming are the enlargement and strengthening of the CG, the strengthening of the NEG, and a flow-direction reversal of the NG. The first two of these occur under all the warming scenarios; the flow-direction reversal occurs only under the +0.1° and +0.2°C scenarios. In the other higher-temperature scenarios, the NG retains its current sense, but enlarges to the north and increases in strength.

Of these three changes, the reversal in direction of the NG under some warming scenarios was not anticipated. In addition to changing direction, this centre of the gyre moves to the north, allowing an area of shear flow to develop between the NG and the CG. However, neither the new position nor the direction reversal of the gyre significantly changed the nature of the cross-boundary flow.

The other two changes in the circulation north of the Central Grounded Zone are the expansion and strengthening of already existing systems. The NEG expands to the south by strengthening existing flow, and towards the CG by eroding further the already weak counter-flow between the two gyres. The CG strengthens to ~0.78 Sv in the +1.0°C case, and expands to the west and northwest, combining with the WBC and the inflow and outflow on the western side of the northern boundary.

The changes in the distribution of melting and freezing between the present conditions and the colder run are insubstantial (Table 1). The changes with the warming runs are more prominent. In most of the domain the direction of change in the melting and freezing rates is the same in each warming scenario. The only exception to this is in the north of the domain, in the area around the NG. In this area different behaviour occurs in the +0.1° and +0.2°C scenarios than in the other warming scenarios.

In the rest of the domain, the warming scenarios all show the same trend. This is illustrated in Figure 4, which shows the difference between the +0.5°C warming scenario and present conditions. In most of the domain we see an increase in the melting rates, or a decrease in the freezing rates (these are both represented by a negative difference). Large rate changes can occur in areas where the melt rate is already strong (Fig. 3). These occur because of the additional heat which reaches these areas from the warmer water circulating in the domain. In turn, the amount of freezing in the small areas increases, as these areas now have an increased supply of supercooled water. However, this has only a local effect as the increased velocities also increase mixing, so the freezing potential is rapidly lost.

In the +0.1° and +0.2°C scenarios, where the NG was found to have shifted further north and reversed direction, three major changes occur. Both the small area of melting around 69.2° S, 70.8° E, and the area of strong freezing

Table 1. Estimates of the mass-balance rates at the base of the Amery Ice Shelf, under colder, present and warmer ocean conditions

	Mean rates of				*Mass accretion rates from*		
	Freezing	*Melting*	*Total*	*Area of melt*	*Freezing*	*Melting*	*Net*
	$m\,a^{-1}$	$m\,a^{-1}$	$m\,a^{-1}$	%	$Gt\,a^{-1}$	$Gt\,a^{-1}$	$Gt\,a^{-1}$
Cooler	0.20	−0.34	−0.13	61.4	3.9	−10.6	−6.7
Present	0.19	−0.36	−0.16	62.4	3.6	−11.4	−7.8
+0.1°C	0.19	−0.42	−0.21	66.1	3.2	−14.1	−10.9
+0.2°C	0.18	−0.48	−0.27	68.9	2.9	−16.7	−13.8
+0.3°C	0.20	−0.58	−0.36	72.0	2.8	−20.9	−18.1
+0.5°C	0.23	−0.69	−0.46	75.7	2.9	−26.4	−23.5
+1.0°C	0.28	−0.87	−0.62	78.6	3.0	−34.6	−31.6

Notes: Positive values indicate mass gain by the ice shelf. The total area of the ice shelf is $5.55 \times 10^4\ km^2$.

https://doi.org/10.3189/1998AoG27-1-75-80 Published online by Cambridge University Press

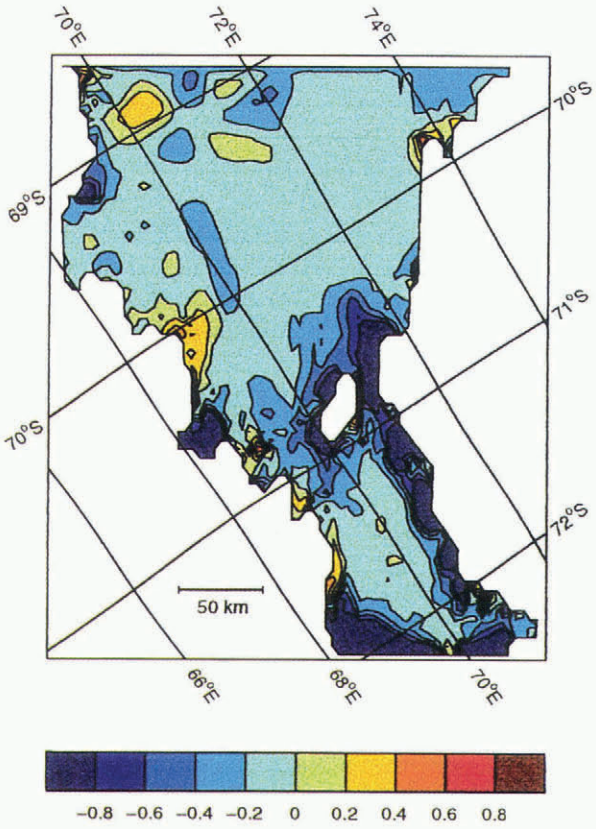

Fig. 4. Change in rates of melting and freezing from present conditions for a 0.5°C temperature increase. Rates are in m a^{-1}, and positive values indicate greater accretion of ice.

around 69.2° S, 72.0° E reduce in strength by a factor of 4, and the area of strong freezing around 68.9° S, 71.2° E, increases in strength and area by a factor of 2. In the other warming scenarios these three areas behave differently. The small area of melting increases its rate of melting by about 0.3 m a^{-1} for the +0.5°C warming case (Fig. 4), and both the areas of freezing decrease their rates of freezing by about 0.4 m a^{-1} for the +0.5°C warming case (Fig. 4). In the +0.3°, +0.5° and +1.0°C warming scenarios we see an increase in the freezing rate around 68.9° S, 70.3° E. This is caused by more supercooled water being carried by the WBC, which is stronger in these warmer runs.

In Table 1 we present several different measures of the change in the basal component of ice-shelf mass balance. The melting rates in the first three columns are the area-averaged rates, over regions where freezing or melting occurs, and for the total ice-shelf area. The next column contains the percentage of the ice-shelf base where melting occurs. For the time rate-of-change in the mass of the ice shelf, the net balance is calculated from the individual melting and freezing rates at the ice-shelf/ocean interface in each model gridcell.

The net amount of ice lost increased in the model runs with warmer boundary temperatures. Most of this change came from increases in both the area of melting and the mean rate of melting, which gave an increase in the gross amount of melting. In contrast, the amount of freezing in the different temperature-change scenarios remained relatively constant. The change with temperature of the total rate of melting and the net amount of melt are ~0.5 m a^{-1} °C^{-1} and ~25 Gt a^{-1} °C^{-1}, respectively.

DISCUSSION AND CONCLUSIONS

Cooling the ocean below present conditions had little effect on either the ocean circulation or the mass balance of the ice shelf. This was because for depths exceeding the minimum ice-shelf draft the mean temperature change was ~−0.03°C, which is evidently insufficient to noticeably affect the circulation. Importantly, it does indicate that if the ocean temperature is generally reduced to the surface freezing point there will still be a net loss of ice by basal melting from the Amery Ice Shelf.

The ocean circulation in the model was affected by warming applied at the northern boundary. The most noticeable small-scale effect was the reversal of the NG, although this reversal disappeared with further warming. In general, the circulation structure became simpler in warmer conditions, with large-scale features becoming more dominant.

Two results which might have been expected from warming the ocean were an increase in the mean melt rates and a decrease in the mean freezing rates. The first of these occurred in all warming scenarios, but the second occurred only in the +0.1° and +0.2°C runs. In the other runs the mean rate of freezing increased for areas where freezing occurred. However, the area of freezing decreased, whereas the area of melting increased. This decrease in area occurs because where freezing is marginal under present conditions, the introduction of warmer waters will change the area from marginal freezing to melting.

The estimates of ice lost through basal melting in this model from present conditions are approximately one-third of those suggested in earlier work. Jacobs and others (1992) estimated the ice lost through basal melting at 23 Gt a^{-1}, with a mean melt rate of 0.65 m a^{-1}. By using computed geostrophic currents based on the observations and conservation of mass, Wong and others (1998) estimated the ice lost by calculating the heat and salt-water fluxes across a hydrographic section in Prydz Bay enclosing the mouth of the cavity under the Amery Ice Shelf. From the separate heat and fresh-water flux balances, they estimated the ice lost at 26 ± 9 and 15 ± 5 Gt a^{-1}, respectively.

The estimate of Jacobs and others (1992) was based on melt-rate estimates from the channel-flow model with seasonal forcing (Hellmer and Jacobs, 1992). The channel-flow model they used approximated a possible two-dimensional "channel" in the three dimensions under the ice shelf. The three-dimensional model suggests that the circulation within the cavity (Fig. 2) is more complicated than the channel-flow model could reasonably be expected to replicate. Hence, it would also seem reasonable to expect that the melt rates predicted by the channel-flow model may overestimate the melting occurring in the ice-shelf cavity.

Two possible explanations are offered for the difference between our estimates and those of Wong and others (1998). The first is that Wong and others calculated the flux through the whole water column, including the part above the cavity and adjacent to the ice-shelf front, using relatively coarsely spaced data compared with our model resolution, collected a short distance from the ice shelf. Accordingly, there is the potential for some of the finer structure of the fluxes to be missed or for additional flux into the water column to occur, for example from melt in the first few km of the ice shelf driven by processes not included in the model (e.g. tidally driven intrusions of warm shelf water). Their oceano-

https://doi.org/10.3189/1998AoG27-1-75-80 Published online by Cambridge University Press

graphic analysis provides an estimate of the net balance of sources of heat and salt flux into the ice-shelf cavity at the ocean front, and suggests that the possibility of fluxes across other boundaries into the cavity should be considered. For example, a possible major source of heat and salt flux not included in our model estimates is from fluxes across the southern boundary of the domain. Recent glaciological studies of ice loss from the Lambert Glacier system suggest that the fresh-water mass flux across the southern boundary of the domain used here may be $\sim$14 Gt a^{-1} (personal communication from A. Ruddell, 1997). Much of this flux could be from small ocean cavities, south of the domain, beyond the resolution capability of this model. Perhaps the most likely explanation for the difference in mass-balance estimates is some combination of these two effects.

With rates of melting and freezing and ice-shelf velocities, it is possible to estimate the cumulative thickness of a marine ice layer along a flowline, including the longitudinal strain, from the continuity equation for a steady-state ice shelf (e.g. Budd and others, 1982). For a flowline running through an area of heavy marine ice accumulation, we found a net marine ice layer of $\sim$162 m formed. This is of similar thickness to the marine ice layer found in the G1 core, from the Amery Ice Shelf, which Morgan (1972) estimated at 158 m thick. This suggests a thick marine ice layer could form over parts of the Amery Ice Shelf, but for a more quantitative comparison the relative transverse-strain thinning of the marine ice layer would also need to be taken into account. For the present model, the flowline through G1 accumulates considerably less marine ice, but uncertainties in the bed topography and ice-shelf draft could account for this.

Nicholls (1997) suggests that the response of the Filchner–Ronne Ice Shelf to warming would be to thicken, i.e. net melting from the ice shelf would decrease, in contrast to our findings for the Amery. In estimating this response, Nicholls assumes that the slight seasonal warming of about 0.1°C is analogous to the effects of climate warming, and that the southern Weddell Sea circulation remains unchanged. Neither of these assumptions is compatible with our model results for the Amery Ice Shelf. We found changes in the ocean circulation as discussed above, and found that in the higher-warming cases the ocean temperatures increase in the south of the domain by about an order of magnitude more than the seasonal change observed by Nicholls. This incompatibility suggests that observed seasonal change may not be a reliable guide for estimating the effects of appreciable climate change under ice shelves.

The severalfold increase in ice mass lost from the base of the Amery Ice Shelf in the model with a 1.0°C increase in water temperature has wide implications for the Lambert Glacier system. With losses due to basal melting approaching the total present input of ice into the ice shelf at the southern boundary of the model, it is to be expected that in reality the ice-shelf geometry would be substantially altered in such a climate-warming scenario. This has implications for grounding-zone retreat and the outflow from the Lambert Glacier, and may have implications for possible increases in melting under warmer conditions for other ice shelves around Antarctica.

ACKNOWLEDGEMENTS

The code for the numerical model was kindly provided by J. Determann, R. Gerdes, and K. Grosfeld of the Alfred-Wegener-Institut für Polar- und Meeresforschung, Bremerhaven, Germany. We would also like to thank them, and I. Allison and N. Bindoff of the Antarctic CRC, for discussions. The hydrographic data were kindly provided by A. Forbes, of the Commonwealth Scientific and Industrial Research Organisation's Division of Marine Research, Hobart.

REFERENCES

Bryan, K. 1969. A numerical method for the study of the circulation of the world ocean. *J. Comput. Phys.*, **14**, 666–673.

Budd, W. F., M. J. Corry and T. H. Jacka. 1982. Results from the Amery Ice Shelf Project. *Ann. Glaciol.*, **3**, 36–41.

Cox, M. D. 1984. *A primitive equation, 3-dimensional model of the ocean.* Princeton, NJ, Princeton University. GFDL Ocean Group. (Technical Report 1.)

Determann, J. and R. Gerdes. 1994. Melting and freezing beneath ice shelves: implications from a three-dimensional ocean-circulation model. *Ann. Glaciol.*, **20**, 413–419.

Determann, J., K. Grosfeld, R. Gerdes and H. Hinze. 1994. Melting and freezing rates beneath Filchner–Ronne Ice Shelf from a 3D-ocean circulation model. *In* Oerter, H., *ed. Filchner–Ronne Ice Shelf Programme. Report 8.* Bremerhaven, Alfred Wegener Institute for Polar and Marine Research, 12–19.

Gerdes, R. 1993. A primitive equation ocean circulation model using a general vertical coordinate transformation. 1. Description and testing of the model. *J. Geophys. Res.*, **98**(C8), 14,683–14,701.

Hellmer, H. H. and S. S. Jacobs. 1992. Ocean interactions with the base of Amery Ice Shelf, Antarctica. *J. Geophys. Res.*, **97**(C12), 20,305–20,317.

Jacobs, S. S., H. H. Hellmer, C. S. M. Doake, A. Jenkins and R. M. Frolich. 1992. Melting of ice shelves and the mass balance of Antarctica. *J. Glaciol.*, **38**(130), 375–387.

Kurinin, R. G. and N. D. Aleshkova. 1987. Korennoy rel'yef Zemli Enderbi, Zemli Mak-Roberstsona i Zemli Printsessy Elizavety v Vostochnoy Antarktide [Bedrock relief of Enderby Land, Mac.Robertson Land and Princess Elizabeth Land, East Antarctica.]. *Antarktika*, **26**, 62–65.

Morgan, V. I. 1972. Oxygen isotope evidence for bottom freezing on the Amery Ice Shelf. *Nature*, **238**(5364), 393–394.

Nicholls, K. W. 1997. Predicted reduction in basal melt rates of an Antarctic ice shelf in a warmer climate. *Nature*, **388**(6641), 460–462.

O'Farrell, S. P., J. L. McGregor, L. D. Rotstayn, W. F. Budd, C. Zweck and R. Warner. 1997. Impact of transient increases in atmospheric CO_2 on the accumulation and mass balance of the Antarctic ice sheet. *Ann. Glaciol.*, **25**, 137–144.

Williams, M. J. M., A. Jenkins and J. Determann. 1998. Physical controls on ocean circulation beneath ice shelves revealed by numerical models. *In* Jacobs, S. S. and R. F. Weiss, *eds. Oceanology, ice and atmosphere: interactions at the Antarctic continental margin.* Washington, DC, American Geophysical Union, 285–300. (Antarctic Research Series 75.)

Wong, A. P. S. 1994. Structure and dynamics of Prydz Bay, Antarctica, as inferred from a summer hydrographic data set. (Master of Polar and Ocean Science thesis, University of Tasmania.)

Wong, A. P. S., N. L. Bindoff and A. Forbes. 1998. On bottom water formation and ocean–ice shelf interaction in Prydz Bay, Antarctica. *In* Jacobs, S. S. and R. F. Weiss, *eds. Ocean, ice and atmosphere: interactions at the Antarctic continental margin.* Washington, DC, American Geophysical Union, 173–188. (Antarctic Research Series 75.)

https://doi.org/10.3189/1998AoG27-1-75-80 Published online by Cambridge University Press